Contribution from the Departments of Chemistry, Ben Gurion University of the Negev, Beer Sheva 84120, Israel, and Bar Ilan University, Ramat Gan, Israel

The Problem of Metal–Metal (MM) Bond Alternation in $[MX_2(\mu\text{-}X)_{4/2}]_\infty$ Chain Polymers

SASON S. SHAIK* and RONY BAR

Received April 29, 1982

The factors that influence MM bond alternation in trans edge-sharing polyoctahedra, $[MX_2(\mu\text{-}X)_{4/2}]_\infty$, are investigated with use of the oligomer M_3X_{14} as a model. The energies of the various oligomers are investigated as a function of the two independent X–M–X equatorial angles. It is shown that the oligomer with the bare core metals, i.e., the d^0–d^0–d^0 case, prefers a structure with two symmetric bridges (equal MM distances) while the d-block electrons tend to prefer asymmetric bridges (unequal MM distances). The analysis leads to one basic principle: *polymers will exhibit MM bond alternation whenever the d-block orbitals are able to take advantage of relatively low energy exit routes in the* $[d^0]_\infty$ *core.* In trans edge-sharing $[MX_2(\mu\text{-}X)_{4/2}]_\infty$ polymers, where X is a donor like a halogen atom, the d-block electrons are stabilized enough by bond alternation and they can take advantage of the shallow walls of the core in this direction. Therefore, all the d counts d^1–d^5 are predicted to exhibit bond alternation. An alternative structure with a uniform but long MM distance is also available for the d^4 and d^5 cases. In d^6 polymers the d-block electrons show no tendency for bond alternation and as a result one expects to find only the structure with a uniform MM distance. *Bond alternation is not a necessary feature of one-dimensional polymers.* It can be circumvented by appropriate design. Thus, substituting the axial ligands by acceptors is expected to generate $[M(CO)_2(\mu\text{-}X)_{4/2}]_\infty$ polymers with uniform, though long, MM distances for the d counts d^1–d^4, d^6, and d^7 or at least to reduce the extent of bond alternation. It is suggested that utilizing bridge ligands with high ligand–ligand overlap repulsion should generate polymers with uniform and short MM distances.

Introduction

Metal halide complexes, MX_n, (n = 1–5), and their derivatives tend to form oligomers and polymers in the solid state[1] as well as in the gas phase.[2] While the higher halides (n = 5) and other five-coordinated complexes of a metal usually form dimers[1,3,4] such as $Nb_2Cl_8(\mu\text{-}Cl)_2$, the lower halides ($n \leq 4$) and complexes with low coordination number form polymers such as $[M(\mu\text{-}X)_{6/2}]_\infty$, $[MX_2(\mu\text{-}X)_{4/2}]_\infty$, etc.[1]

The aggregation motifs of these complexes with the low coordination number are numerous and thereby generate a spectrum of possible isomeric polymers with a fascinating molecular architecture.[1,5] The most well-known and probably the simplest motif arises from polymerization of MX_4 units to a chain of MX_6 octahedra sharing trans edges, $[MX_2(\mu\text{-}X)_{4/2}]_\infty$ (**1**).

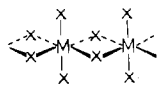

1 $[MX_2(\mu\text{-}X)_{4/2}]_\infty$

However, even within this simple and relatively small subset of polymers there are different structural choices. Depending on the nature of M, the known polymers either have alternating, long–short, MM distances (**2**) such as in $[NbI_2(\mu\text{-}I)_{4/2}]_\infty$[6] or a uniform MM distance (**3**) as in $[OsCl_2(\mu\text{-}Cl)_{4/2}]_\infty$.[7]

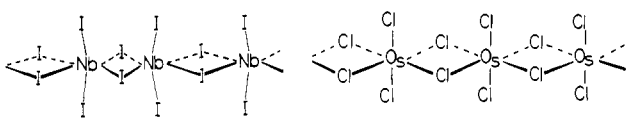

r_{MM}(Å) = 3.31, 4.36 2 r_{MM}(Å) = 3.56 3

Due to their extended chain structures, these compounds are considered as potential one-dimensional conductors.[1c,8] But as such, the propensity of many of them toward bond alternation prevents any chances for appreciable conductivity.

The problem of bond alternation occupies a unique place in chemistry and in physics. It seems to be an inherent property of many one-dimensional organic (e.g., polyenes) as well as inorganic polymers and thereby diffuses some of the hope of designing efficient one-dimensional conductors. Therefore, it is important to analyze the factors that cause bond alternation and to attempt an understanding of how to remedy the problem. Thus, our general goal is to investigate the factors that dominate the structural features of the polymers (**1**) with an aim to provide an insight that we hope may prove useful for the synthetic effort in this area.

Our questions concern the nature of the metal–bridging-ligand interaction, the metal–metal interaction, and the role of the metal d count in dictating structural preferences. In short, we are asking the following question: Why do some polymers alternate while others do not?

Strategy and Method

Whereas physical properties, e.g., conductivity, of the polymer $[MX_2(\mu\text{-}X)_{4/2}]_\infty$ must be deduced from calculations

* To whom correspondence should be addressed at Ben Gurion University of the Negev.

(1) For general reviews see: (a) Gutman, V., Ed. "Halogen Chemistry"; Academic Press: New York, 1967; Vol. 3. (b) Schäfer, H.; Schnering, H. G. *Angew. Chem.* **1964**, *76*, 833. (c) Stucky, G. D.; Schultz, A. J.; Williams, J. M. *Annu. Rev. Mater. Sci.* **1977**, *7*, 301. (d) Corbett, J. D. *Acc. Chem. Res.* **1981**, *14*, 239. (e) Vahrenkamp, H. *Angew. Chem., Int. Ed. Engl.* **1978**, *17*, 379. (f) Spivack, B.; Dori, Z. *Coord. Chem. Rev.* **1975**, *17*, 99. (g) Wycoff, R. W. "Crystal Structures"; Wiley-Interscience: New York, 1965; Vols. 1–3.
(2) Schäfer, H. *Angew. Chem., Int. Ed. Engl.* **1976**, *12*, 713.
(3) The following is just a representative small list of dimers: (a) Zalkin, A.; Sands, D. E. *Acta Crystallogr.* **1958**, *11*, 615. (b) Sands, D. E.; Zalkin, A. *Ibid.* **1959**, *12*, 723. (c) Dahl, L. F.; Wampler, D. L. *J. Am. Chem. Soc.* **1959**, *81*, 3150. (d) Mucker, K.; Smith, G. S.; Johnson, Q. *Acta Crystallogr., Sect. B* **1968**, *B24*, 874. (e) Mimry, T.; Walton, R. A. *Inorg. Chem.* **1977**, *16*, 2829. (f) Jackson, R. B.; Streib, W. E. *Ibid.* **1971**, *10*, 1760. (g) Saillant, R.; Hayden, J. L.; Wentworth, R. A. D. *Ibid.* **1967**, *8*, 1497.
(4) See, however, higher aggregates for NbF_5, TaF_5, etc.: Edwards, A. J. *J. Chem. Soc.* **1964**, 3714.
(5) See, for example, the isomers of MnP_4: (a) Jeitschko, W.; Rühl, R.; Krieger, U.; Heiden, C. *Mater. Res. Bull.* **1980**, *15*, 1755. (b) Rühl, R.; Jeitschko, W. *Acta Crystallogr., Sect. B* **1981**, *B37*, 39. (c) Jeitschko, W.; Donohue, P. C. *Ibid.* **1975**, *B31*, 574.
(6) (a) Dahl, L. F.; Wampler, D. L. *Acta Crystallogr.* **1962**, *15*, 903. (b) Seabaugh, P. W.; Corbett, J. D. *Inorg. Chem.* **1965**, *4*, 176. (c) Corbett, J. D.; Seabaugh, P. W. *J. Inorg. Nucl. Chem.* **1958**, *6*, 207.
(7) Cotton, F. A.; Rice, C. E. *Inorg. Chem.* **1977**, *16*, 1865.
(8) (a) Kepert, D. L.; Marshall, R. E. *J. Less-Common Met.* **1974**, *34*, 153. (b) Kawamura, H.; Shirotani, I.; Tachikawa, K. *Phys. Lett. A* **1978**, *65A*, 335. (c) Kawamura, H.; Shirotani, I.; Tachikawa, K. *J. Solid State Chem.* **1979**, *27*, 223.

0020-1669/83/1322-0735$01.50/0

that take into account the infinite dimension of the chain,[9] gross structural features such as bond alternation can be understood by studying smaller segments.[10] This, in fact, becomes a necessity if one wishes, as we do, to study the geometric features in great detail. Therefore, we have chosen as a possible model the smallest oligomer, M_3X_{14} (**4**), that can exhibit a nonuniform MM distance.

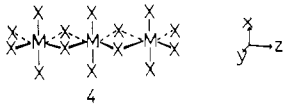

4

The focus of MM bond alternation and metal–metal bonding is in the inner bridge rhomboids. Therefore, we have optimized the geometry of the oligomer (**4**) with respect to the angles θ_1 and θ_2 (**5**), which were allowed to vary inde-

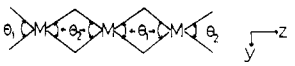

5

pendently over the range 70–100°. The alternation in the outer nonrhomboid angles acts as a constraint that mimics the state of the oligomer within the polymer.

Thus, $\theta_1 \neq \theta_2$ is an indicator of unequal MM distances and hereafter will be referred to as "bond alternation" although the term is not adequate for the oligomer. The values of θ_1 and θ_2 provide further information about the individual MM distances and magnitude of metal–metal interactions.[11]

Our model compound for **4** is $[Nb_3Cl_{14}]^Z$ with Z = 1+, 2–, 5–, 8–, 11–, 14–, 17–. The variable charge serves to control the d count on the metals, thereby modeling different metals. If the usual d-electron bookeeping is followed, Z = 0 leaves one d electron for the Nb_3Cl_{14} moiety, and hence, Z = 1+ corresponds to a case of zero d electrons. This case, Z = 1+, will be designated as a d^0–d^0–d^0 compound. It follows that Z = 2–, 5–, 8–, 11–, 14–, and 17– correspond respectively to d^n–d^n–d^n compounds with n varying from 2 to 6. These cases together will serve to model the range of d counts found in the various existing polymers,[1] beginning with $[NbX_2(\mu\text{-}X)_{4/2}]_\infty$ (X = halide) all the way to $[PtX_2(\mu\text{-}X)_{4/2}]_\infty$, which span the range of $[d^1]_\infty$ to $[d^6]_\infty$.

Our method of calculation is of the extended Hückel type with the parameters given in the Appendix. This method has already been useful in studying metal–metal bonding,[12a–d] bridged compounds,[11a–c] and band structure[9a,10,12e,f] in a wide variety of organometallic and inorganic compounds.[13] Though it has well-recognized deficiencies, its lucid nature allows us to construct a comprehensive scheme and to conceptualize a wide range of molecules, and this is what we aim for in this paper.

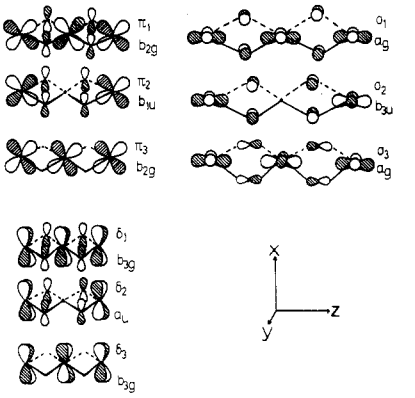

Figure 1. The nine lower d-block orbitals of M_3Cl_{14} arranged in sets of σ, π, and δ type MOs.

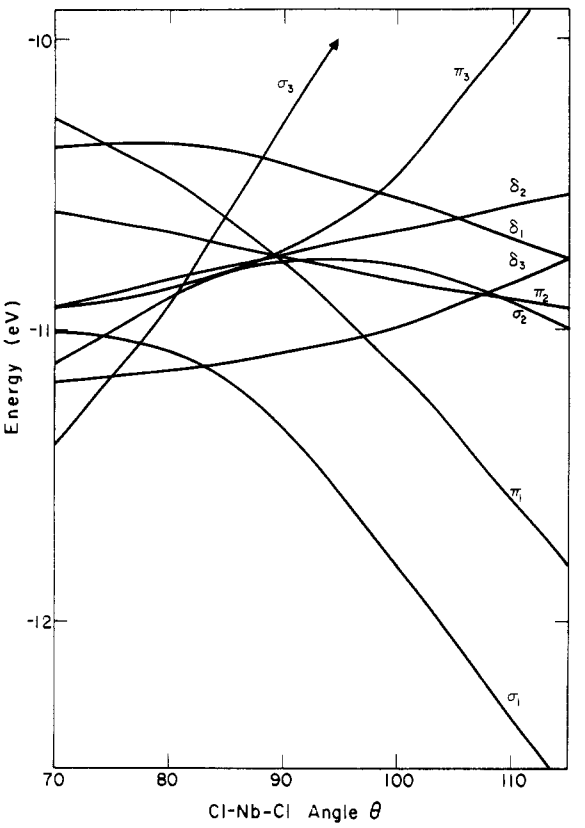

Figure 2. Energy variation of the d-block orbitals of Nb_3Cl_{14} as a function of θ in the symmetric distortion ($\theta_1 = \theta_2$).

Results for $[Nb_3Cl_{14}]^Z$

A. d-Block Orbitals. Our first query is concerned with the role of the d electrons in establishing geometric preferences and in realizing potential metal–metal bonding. The familiar three below two splitting of the d orbitals in the monomer[14] becomes nine below six in the trimer. The nine lower lying orbitals of a trimer with equal MM distances in a D_{2h} symmetry are shown in Figure 1, with omission of the axial and the terminal contributions.

The upper six orbitals, which are not shown in the Figure, lie in our calculations 3–4 eV higher and therefore are not likely to be accessible for electron occupancy. This limits the highest possible d count to d^6–d^6–d^6, which leads to a full occupancy of the nine orbitals.

(9) The band structure of NbX_4 chains is calculated in: (a) Whangbo, M.-H.; Foshee, M. J. *Inorg. Chem.* **1981**, *20*, 118. (b) Bullett, D. W. *Ibid.* **1980**, *19*, 1780. (c) Reference 1c.

(10) See, for example: (a) Hoffmann, R.; Shaik, S.; Scott, J. C.; Whangbo, M.-H.; Foshee, M. J. *J. Solid State Chem.* **1981**, *34*, 263. (b) Burdett, J. K. *J. Am. Chem. Soc.* **1980**, *102*, 450.

(11) For a similar approach see: (a) Summerville, R. H.; Hoffmann, R. *J. Am. Chem. Soc.* **1976**, *98*, 7240. (b) *Ibid.* **1979**, *101*, 3821. (c) Shaik, S.; Hoffmann, R.; Fisel, R. C.; Summerville, R. H. *Ibid.* **1980**, *102*, 4555. (d) Dahl, L. F.; Rodulfo de Gil, E.; Feltham, R. D. *Ibid.* **1969**, *91*, 1653. (e) Cotton, F. A.; Ucko, D. A. *Inorg. Chim. Acta* **1972**, *6*, 161. (f) Burdett, J. K. *J. Am. Chem. Soc.* **1979**, *101*, 5217.

(12) (a) Hay, P. J.; Thibeault, J. C.; Hoffmann, R. *J. Am. Chem. Soc.* **1975**, *97*, 4884. (b) Lauher, J. W.; Elian, M.; Summerville, R. H.; Hoffmann, R. *Ibid.* **1976**, *98*, 3219. (c) Albright, T. A.; Hoffmann, R. *Ibid.* **1978**, *100*, 7736. (d) Dedieu, A.; Albright, T. A.; Hoffmann, R. *Ibid.* **1979**, *101*, 3141. (e) Whangbo, M.-H.; Hoffmann, R. *Ibid.* **1978**, *100*, 6093. (f) Whangbo, M.-H.; Foshee, M.; Hoffmann, R. *Inorg. Chem.* **1980**, *19*, 1723.

(13) For a review, see: Albright, T. A. *Tetrahedron, Rep.*, in press.

(14) (a) Elian, M.; Hoffmann, R. *Inorg. Chem.* **1975**, *14*, 1058. (b) Albright, T. A.; Hoffmann, R.; Thibeault, J. C.; Thorn, D. L. *J. Am. Chem. Soc.* **1979**, *101*, 3801. (c) Hoffmann, R. *Science (Washington, D.C.)* **1981**, *211*, 995.

This nest of orbitals in the figure is composed of three triads belonging to σ, π, and δ types in their bonding characteristics. In our coordinate system the σ type orbitals are made of $z^2 - y^2$ metal d orbitals and the π type orbitals of xz metal d orbitals, while the δ type orbitals are made of xy metal d orbitals.

The orbital subscripts designate the nodal properties with respect to the metal–metal axis. The subscript 1 (e.g., σ_1) stands for zero nodes between the metals and, therefore, for maximum metal–metal bonding, whereas 3 (e.g., σ_3) stands for the maximal number of nodes and, therefore, maximum metal–metal antibonding. The σ_2 and π_2 orbitals actually contain also a contribution from p_z and p_x orbitals on the central metal atom. However, this contribution is so minute that it can be disregarded and therefore is not shown in Figure 1.

Since we are interested in structures that exhibit bond alternation ($\theta_1 \neq \theta_2$ in **4**) as well as in structures that have a uniform MM distance ($\theta_1 = \theta_2$), we must investigate the behavior of the d-block orbitals under these two structural variations. Figure 2 shows a Walsh diagram of the nine d orbitals of Nb_3Cl_{14} upon a symmetric distortion that maintains $\theta_1 = \theta_2$ (**4**) over the range 70–110°.

The energy variation of the orbitals is in accord with their MM bonding characteristics. Thus the maximum MM bonding orbitals, especially σ_1 and π_1, descend in energy as θ increases (MM distances decrease) in rates that correspond to their MM overlap type characteristics. Similarly the maximum MM antibonding orbitals σ_3, π_3, and δ_3 rise up in energy with increasing θ, whereas σ_2, π_2, and δ_2 remain relatively flat. This pattern creates two distinct regimes. The low-θ regime is characterized by an antibonding below bonding orbital pattern (e.g., σ_3 below σ_1). This is a region where no metal–metal bonding can be established and the ordering of the d levels is set by their coupling with the bridging ligand orbitals.

The second region is the regime of large θ. In this region the level ordering obeys the expected through-space pattern with MM bonding and nonbonding orbitals being below the corresponding antibonding orbitals. If this region can become energetically accessible, then metal–metal bonding will be realized in the d counts d^n–d^n–d^n, n = 1–5.

Clearly, the level ordering of the d-block orbitals obtains from a fine balance between the MM through-space interaction and the coupling with bridging ligands. Therefore, we turn now to piece up these MOs from their building-block components in a manner that can reveal this balance. The piecing-up process is shown schematically in **6**.

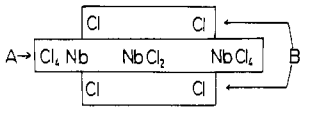

6

The first fragment (A) contains the metal chain including all the axial chlorines and the terminal equatorial chlorines, while the second fragment (B) contains the four bridging chlorines only. Fragment A can itself be pieced up by flanking the central $NbCl_2$ unit with two $NbCl_4$ units. The construction of the d-block orbitals of Nb_2Cl_8 is straightforward,[11c] and the six lower orbitals of the unit are shown on the right-hand side of Figure 3. These are the bonding and antibonding (starred) pairs of the σ, π, and δ varieties. The coupling of these orbitals with the corresponding σ, π, and δ orbitals of the central $NbCl_2$ moiety generates the lower d-block orbitals of Nb_3Cl_{10} (fragment A), which are shown in the center of Figure 3.

Three of the Nb_2Cl_8 orbitals, σ^*, δ^*, and π, do not find a match with d orbitals on $NbCl_2$, thus forming the σ_2, π_2, and δ_2 triad of Nb_3Cl_{10}. The remaining three orbitals of Nb_2Cl_8,

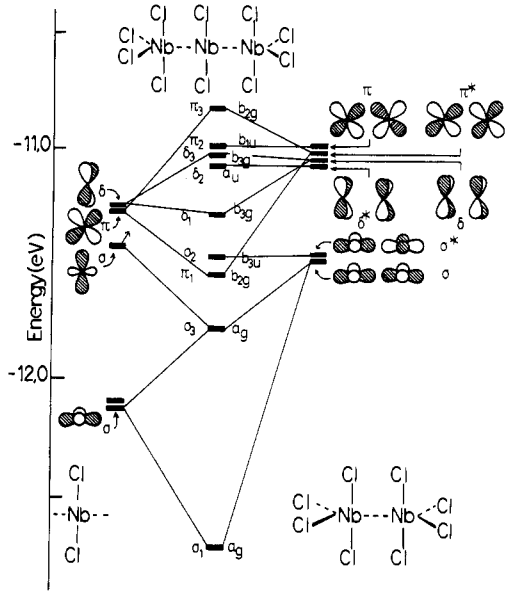

Figure 3. Interaction diagram describing the construction of the d orbitals of Nb_3Cl_{10} (fragment A) from the fragment orbitals of Nb_2Cl_8 and $NbCl_2$. NbNb distances correspond to θ = 90°.

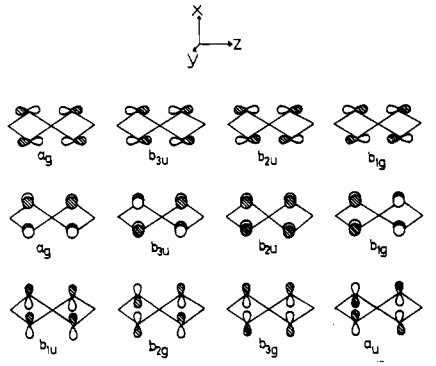

Figure 4. Orbitals of the bridging unit $(Cl)_4$. Only the orbitals that are made from the p AOs are shown.

σ, δ, and π^*, interact with the corresponding σ, δ, and π orbitals of $NbCl_2$ and thereby generate the σ_1, σ_3, δ_1, δ_3, and π_1, π_3 orbital pairs of Nb_3Cl_{10}.

The d-block orbitals of fragment A (Nb_3Cl_{10}) so resulting span quite a wide range of energy (≥2 eV), and the level ordering within each set generally obeys the through-space coupling, e.g., $E(\pi_1) < E(\pi_2) < E(\pi_3)$. The only exception occurs in the σ set, where σ_2 and σ_3 reverse their expected normal order. This reversal originates in the three-orbital interaction, which depresses the level of σ_3 (Figure 3), but the normal through-space ordering will be restored at larger θ values (shorter NbNb distances).

The MOs of the bridging unit (B) are shown in Figure 4 with D_{2h} symmetry labels. The final step of the mosaic consists of piecing together fragments A and B. A simplified version of the interaction diagram is shown in Figure 5. The nine d-block orbitals of Nb_3Cl_{10} all find a symmetry match with the orbitals of the coupling unit $(Cl)_4$ and thus interact to form the nine d-block orbitals of Nb_3Cl_{14} (Figure 1). As a result of the various orbital interactions the through-space level ordering established in Nb_3Cl_{10} is completely destroyed; π_1 is raised above π_2 and π_3 and likewise δ_1 is raised above δ_2 and δ_3, and the entire d block is condensed in energy (to ~0.6 eV).

Figure 5 clearly shows that the level ordering is an outcome of the interplay between the through-space interaction and the bridge coupling. We can now discuss, in the light of the figure, the variation in this interplay upon changes in θ. We begin with the π set. The interacting fragment orbitals of Nb_3Cl_{10}

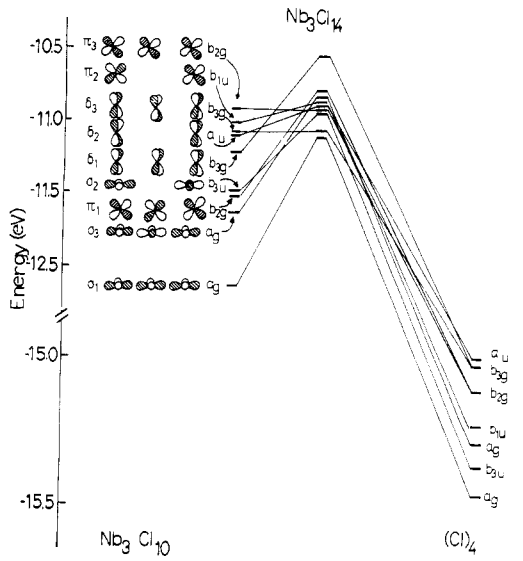

Figure 5. Interaction diagram describing the construction of the d-block orbitals of Nb_3Cl_{14} from the fragment orbitals of Nb_3Cl_{10} and those of the bridging unit $(Cl)_4$. Note the energy scale for the bridging unit is different than that of Nb_3Cl_{10}. The level ordering corresponds to $\theta = 90°$.

and $(Cl)_4$ are drawn in *one* of the rhomboid sections (**7–9**), with the respective fragment orbital overlaps.

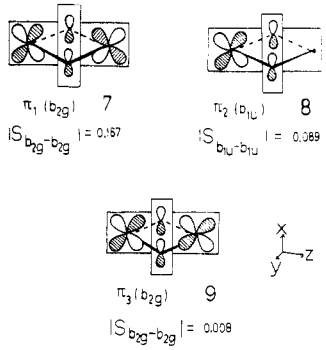

In the case of π_1 the two xz metal orbitals at the corners of each rhomboid are in phase and therefore overlap with the x fragment orbital of $(Cl)_4$ in a reinforcing manner, leading to a large overlap (**7**). On the other hand, the fragment orbital overlap is close to zero (**9**) for π_3, where the out-of-phase relation of the metal xz orbitals, at the rhomboid corners, results in a mutual cancellation of the overlap with the x fragment orbital of $(Cl)_4$. π_2 is an intermediate case (**8**), which involves an intermediate overlap owing to the node at the central metal.

At small θ, when the through-space MM interaction is weak, the coupling with the ligands wins out and inverts the natural level ordering (**10**). At large θ the through-space interaction

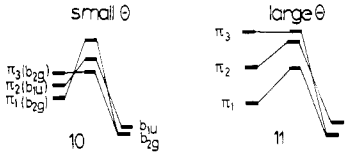

is strong enough to retain the normal order, $E(\pi_1) < E(\pi_2) < E(\pi_3)$ (**11**).

Analogous considerations apply to the δ set of orbitals. However, since the through-space interaction of the xy metal orbitals remains quite small throughout the range of θ, the normal level ordering of δ_1, δ_2, and δ_3 is not fully restored even at $\theta = 110°$, and the level pattern remains controlled by the coupling with the bridge ligands.

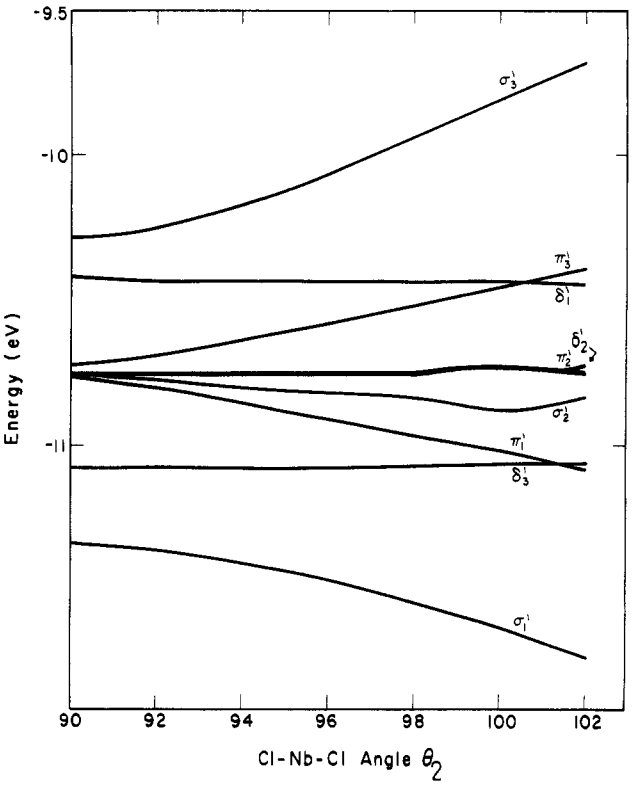

Figure 6. Energy variation of the d-block orbitals of Nb_3Cl_{14} as a function of θ_2 ($\theta_1 = 90°$ throughout) in the asymmetric distortion ($\theta_1 \neq \theta_2$).

The σ set exhibits a different interaction pattern. Here, both $\sigma_1(Nb_3Cl_{10})$ and $\sigma_3(Nb_3Cl_{10})$ interact strongly with a_g type orbitals of $(Cl)_4$; σ_1 interacts with the y type orbital, whereas σ_3 interacts with the z type orbital. As shown in **12** and **13**,

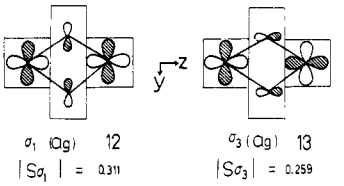

the overlap of σ_1 is larger than that of σ_3. The remaining member of the set, σ_2, interacts with the b_{3u} orbital of $(Cl)_4$, and its interaction is weaker than those of either σ_1 or σ_3. This order in the fragment MO overlaps, $|S(\sigma_1)| > |S(\sigma_3)| > |S(\sigma_2)|$, sets the level ordering. At low θ, the through-space ordering $E(\sigma_1) < E(\sigma_3) < E(\sigma_2)$ established in Nb_3Cl_{10} (fragment A) becomes $E(\sigma_3) < E(\sigma_2) < E(\sigma_1)$, by coupling with the bridging ligands (**14**), while at high θ, the strong through-space interaction wins out and restores the normal order, $E(\sigma_1) < E(\sigma_2) < E(\sigma_3)$ (**15**).

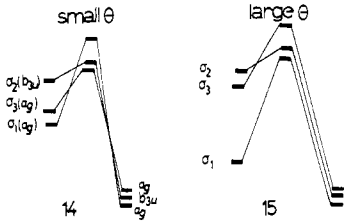

The behavior of the d-block orbitals upon a symmetric distortion ($\theta_1 = \theta_2$) over a wide range of θ is now fairly clear. Our next step is to consider the influence of an asymmetric distortion, one that leads to $\theta_1 \neq \theta_2$ (**5**), on the energy of the d orbitals. A Walsh diagram that shows the energies of the

nine d orbitals as a function of θ_2 in the range of 90–102°, where θ_1 remains constant at 90°, is shown in Figure 6. The figure exhibits a general pattern. The asymmetric distortion leads to large stabilization of the fully bonding orbitals σ_1' and π_1' and to a large destabilization of the antibonding orbitals σ_3' and π_3', while the nonbonding orbitals σ_2' and π_2' remain relatively flat.

This pattern results from an intraset orbital remixing. Let us describe the effect with the σ set as an example. In D_{2h} the distortion mode that leads to $\theta_1 \neq \theta_2$ (**5**) behaves like the irreducible representation b_{3u}, i.e., like the z axis. Therefore the orbital pairs that will interact with each other strongly under the distortion are those whose direct product matches the symmetry of the distortion. These pairs are σ_1–σ_2 and σ_3–σ_2.[15] As a result of these mixings, σ_1' and σ_3' (after interaction) become more like σ and σ^* of the short MM linkage and begin to resemble the building blocks of the σ band in the polymer as was nicely described by Whangbo[9a] and by Bullett.[9b] This is shown in **16** for σ_1'.

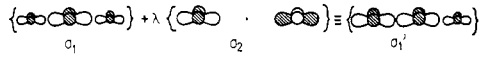

16

The energy ordering at the origin of the distortion ($\theta_1 = \theta_2 = 90°$) is $E(\sigma_1) < E(\sigma_2) < E(\sigma_3)$ as shown in Figures 2 and 6. Consequently, σ_2 is sandwiched from below and above by its interactions with σ_1 and σ_3; thus, its energy remains relatively unchanged throughout the distortion. At the same time, σ_1 is stabilized while σ_3 is destabilized by their interactions with σ_2, as shown in **17** (double-headed arrows mark interactions).

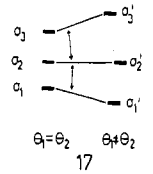

17

Analogous conclusions apply to the π set. On the other hand, the δ set is somewhat different. Since the intraset interactions are proportional to the overlaps of the d AOs on the metals that approach one another,[15] the δ set, having a weak AO overlap, is hardly affected by the distortion and the three δ orbitals, δ_1, δ_2, and δ_3, barely change in energy upon distortion.

B. Core Energy. At this point we have a detailed picture of the behavior of the d-block orbitals upon the possible distortions that the molecular framework can experience. This information is vital since these orbitals will be occupied by the metals' d electrons, which can buttress the molecular framework with metal–metal bonding.

From the Walsh diagrams in Figures 2 and 6 one would have expected more or less a uniform behavior for all the d counts from d^1–d^1–d^1 to d^5–d^5–d^5, *if the d orbitals were domineering*. On this premise, the d^1–d^1–d^1 case should exhibit bond alternation and find an energy minimum in a structure with one very large angle, thus stabilizing the $(\sigma_1')^2(\pi_1')^1$ configuration. Similarly d^2–d^2–d^2, d^3–d^3–d^3, and d^4–d^4–d^4 should favor bond alternation with one very large angle stabilizing respectively the electronic configurations $(\sigma_1')^2(\pi_1')^2(\delta_3')^2$, $(\sigma_1')^2(\pi_1')^2(\delta_3')^2(\sigma_2')^2(\pi_2')^1$, and $(\sigma_1')^2(\pi_1')^2(\delta_3')^2(\sigma_2')^2(\pi_2')^2(\delta_2')^2$. The d^5–d^5–d^5 case should favor bond alternation too, but with a smaller difference between the angles, since now one starts populating the uprising antibonding orbital π_3'. In all these cases one would have expected net metal–metal bonding with a maximum capacity of two bonds for the entire molecule (for n = 2–5).

From our experience[11c] we knew that this premise is not always valid and there are other important factors that could dominate the structural variations. Therefore, we have optimized the geometries for all the d counts d^n–d^n–d^n (n = 1–6) with respect to θ_1 and θ_2. The angles were allowed to vary independently. The results are shown in Table I.

Table I. Optimum Angles (θ_1, θ_2) for d^n–d^n–d^n (n = 1–6) Configurations of $[Nb_3Cl_{14}]^{2-}$

n	θ_1 (r_1)[a]	θ_2 (r_2)[a]	electronic config
1	92 (3.44)	84 (3.68)	$(\sigma_1')^2(\delta_3')^1$
2	98 (3.25)	80 (3.79)	$(\sigma_1')^2(\delta_3')^2(\pi_1')^2$
3	95 (3.34)	79 (3.82)	$(\sigma_1')^2(\delta_3')^2(\pi_1')^2(\sigma_2')^2(\delta_2')^1$
4	80 (3.79)	80 (3.79)	$\delta_3^2\sigma_1^2\sigma_3^2\sigma_2^2\pi_3^2\delta_3^2$
	97 (3.28)	80 (3.79)	$(\sigma_1')^2(\delta_3')^2(\pi_1')^2(\sigma_2')(\delta_2')^2(\pi_2')^2$
5	79 (3.82)	79 (3.82)	$\delta_3^2\sigma_1^2\sigma_3^2\sigma_2^2\pi_3^2\delta_2^2\pi_2^2\pi_1^1$
	93 (3.41)	82 (3.73)	$(\sigma_1')^2(\delta_3')^2(\pi_1')^2(\sigma_2')^2(\delta_2')^2(\pi_2')^2$-$(\pi_3')^2(\delta_1')^1$
6	81 (3.76)	81 (3.76)	$\delta_3^2\sigma_1^2\sigma_3^2\sigma_2^2\pi_3^2\delta_2^2\pi_2^2\pi_1^2\delta_1^2$

[a] θ in degrees, r in Å. The r's are MM distances.

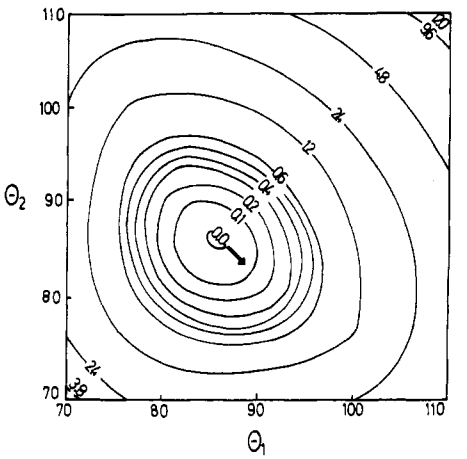

Figure 7. Energy of the core, d^0–d^0–d^0, for $(Nb_3Cl_{14})^+$ as a function of the angles θ_1 and θ_2. Energy contours are in eV.

The table reveals that, although the d^n–d^n–d^n complexes with n = 1–5 indeed find minima in asymmetric structures with $\theta_1 \neq \theta_2$, the d orbitals alone are not telling us all the story. There are other constraints that act to undo the tendencies imposed by the d block. Especially interesting are the d^4–d^4–d^4 and d^5–d^5–d^5 cases, which each exhibit a double minimum, one with $\theta_1 = \theta_2$ and the other with $\theta_1 \neq \theta_2$.

How can we account for these findings? Within the EH method the total energy can be thought of as being composed of the d-block energy and that of all the other electrons which occupy the low-lying metal–ligand bonding orbitals and ligand nonbonding orbitals.[11a-c,14] Whereas the d block tends to push the molecular framework toward geometries where metal–metal bonding is strong, the block of lower lying orbitals forms *a core* that constrains the molecular framework from establishing such geometries.

The core is the d^0–d^0–d^0 case, which has no d electrons. The potential energy sheet at the range of θ = 70–110° is shown in Figure 7 for $[Nb_3Cl_{14}]^+$, which simulates the d^0–d^0–d^0 core for our trimer. The energy sheet of d^0–d^0–d^0 spreads like a hammock whose highest anchor point is at $\theta_1 = \theta_2 = 110°$, 12 eV above the lowest point at $\theta_1 = \theta_2 \approx 86°$. The second

(15) This can also be deduced from MO overlap considerations. The overlap of σ_1 and σ_3 is $2a^2S_{AC}$, where a is the AO coefficient of the first and the third metal atoms A and C, respectively. The AC distance is large (≥7 Å), and hence $S_{AC} \sim 0$ and the σ_1–σ_3 interaction is small. The σ_1–σ_2 overlap is $b^2(S_{AB} - S_{BC})$, where B is the central atom. Since the AB distance shrinks while the BC distance increases upon distortion, the σ_1–σ_2 overlap increases and so does the respective orbital interaction. The same applies to σ_3–σ_2. We have verified this conclusion by reexpressing σ_1', σ_2', and σ_3' in terms of σ_1, σ_2, and σ_3.

anchor point at $\theta_1 = \theta_2 = 70°$ is much lower, at ~3.8 eV above the minimum. The belly of the hammock, about the minimum, is eye-shaped and is elongated in a direction along which $\theta_1 \neq \theta_2$, as shown by the arrow in Figure 7.

Two factors contribute to these features of the d^0–d^0–d^0 sheet, much the same as they did in the case of the edge-sharing bioctahedra M_2L_{10}, which we discussed previously.[11c] The shape of the hammock away from its belly is dominated mainly by the axial ligand–ligand overlap repulsion due to the lone pairs pointing toward each other as shown in **18** and **19**. This is really a steric effect within the EH method.

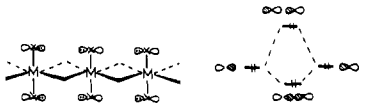

18 19

If we start our excursion from the d^0–d^0–d^0 minimum (Figure 7) and perform a symmetric, $\theta_1 = \theta_2$, squeeze, then six axial chlorines will be approaching one another. As a result, the overlap of the axial ligand lone pairs will increase, leading to increasing overlap repulsion and to a steep energy rise, which dominates the position of the upper anchor point at $\theta_1 = \theta_2 = 110°$ in Figure 7. This sharp energy rise of the d^0–d^0–d^0 curve can indeed be mimicked nicely by six chloride ions whose positions are varied the same as those of the axial chlorines (**18**) along the $\theta_1 = \theta_2$ distortion.

Starting the excursion along the arrow in Figure 7 will cause an approach of only four axial chlorines, whereas the other two will move away from the rest. Therefore, the rising wings of the hammock in the $\theta_1 \neq \theta_2$ direction are much less steep than in the $\theta_1 = \theta_2$ direction. This is the reason for the eye-shaped belly in Figure 7. Thus, *the tempered steric effect (overlap repulsion) in the $\theta_1 \neq \theta_2$ direction provides the molecular framework with a possible exit route from the d^0–d^0–d^0 minimum.*

The other factors that play a key role in setting the features of the d^0–d^0–d^0 core are the bridge bonding and the bridge ligand–ligand overlap repulsion.[16b] Together, these two determine the strength of the ligand–metal bridge bonds and the location of the d^0–d^0–d^0 minimum.

As we have reasoned before,[11c] the bridge bonding reflects the donor–acceptor interaction between the bridging ligand, which is equipped with a lone-pair orbital and acts as a donor, and the metal moiety, which is equipped with low-lying empty orbitals and acts as an acceptor. This is shown pictorially in **20**.

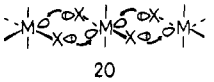

20

This donor–acceptor relationship is in fact manifested in the existence of $[d^0]_\infty$ polymers like $[ZrCl_2(\mu\text{-}Cl)_{4/2}]_\infty$,[17] $(d^0)_4$ tetramers like $[NbF_5]_4$,[4] and a multitude of d^0–d^0 dimers in the gas phase, in the solid phase, and in solution.[1-3]

As the bridging ligand is made a better electron donor and the metal moiety a better acceptor, one expects the d^0–d^0–d^0 trimer (or, in general, polymer) to have stronger bridge bonding and therefore to be more stable. In our search in Figure 7, this can be estimated by the depth of the minimum (~4 eV) relative to $\theta_1 = \theta_2 = 70°$.[11c]

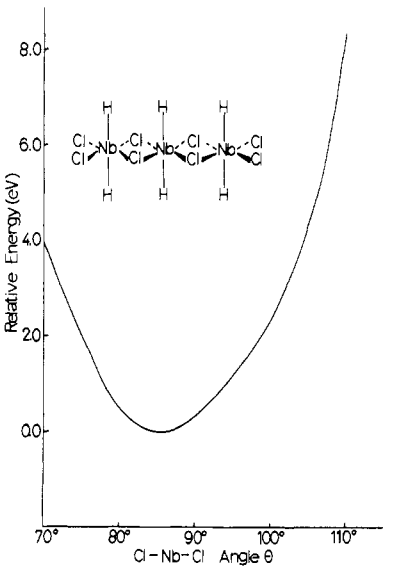

Figure 8. Energy of the core, d^0–d^0–d^0, for $(Nb_3H_6Cl_8)^+$ as a function of the angle θ in the symmetric distortion ($\theta_1 = \theta_2$).

The location of the minimum is dominated by the overlap repulsion of the bridging ligand lone pairs, which point toward each other (**21**). This interaction will prefer to open the angle

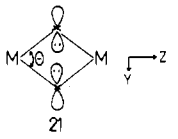

21

θ (**21**) and to fix a compromised minimum, which relieves this strong repulsion.[11c,16b]

Thus, as much as one can separate the effects, we can conclude that the depth of the d^0–d^0–d^0 minimum and its location are determined by the bridges, while the rising walls beyond the minima are determined by axial ligand–ligand interactions. To verify these guidlines, we have calculated the d^0–d^0–d^0 minimum of $[Nb_3Cl_8H_6]^+$, in which all the axial chlorines were replaced by the sterically less demanding hydrogens. The energy curve along $\theta_1 = \theta_2$ is shown in Figure 8. One can see that replacing the axial chlorines only tempers the energy rise and sets the high-energy point ($\theta_1 = \theta_2 = 110°$) at ~8 eV relative to the minimum in comparison with ~12 eV in Figure 7. The other features, the location of the minimum (~86°) and its depth relative to $\theta_1 = \theta_2 = 70°$, as expected, remain unchanged.

In conclusion, the d^0–d^0–d^0 core prefers an undistorted structure with $\theta_1 = \theta_2 \sim 86°$. The molecule inside this energy well *has only one relatively easy mode of escape, in a $\theta_1 \neq \theta_2$ direction (Figure 7), which leads to bond alternation.* On the other hand, distortion along the $\theta_1 = \theta_2$ direction ($\theta > 86°$) is barred by the sharp energy rise in this direction.

Structural changes can be induced by populating the d-block orbitals which show a marked propensity for distorting in the $\theta_1 \neq \theta_2$ direction (Figure 6). *This propensity, together with the relative ease of escape in the $\theta_1 \neq \theta_2$ direction (Figure 7) combine to generate low-spin structures with bond alternation for d^n–d^n–d^n, n = 1–5 (Table I).*

The tendency of the d block for bond alternation will be tempered by the rising energy walls of the core (Figure 7). Thus, as the $\theta_1 - \theta_2$ difference increases, the increasingly stabilizing d-block energy will be balanced out by the increasingly destabilizing core energy (consult Figure 7).[16a] The outcome is a small variation in the degree of bond alternation as a function of the d count, as witnessed by the results in Table I.

(16) (a) Our calculations utilize perpendicular M–X axial bonds (e.g., **4**). As suggested by a reviewer, the tilting of the axial ligands away from their perpendicular direction (as, e.g., in **2**) is expected to further temper the steepness of the d^0–d^0–d^0 curve in the $\theta_1 \neq \theta_2$ direction. (b) For the role of bridge ligand–ligand interactions, see: Ross, F. K.; Stucky, G. D. *J. Am. chem. Soc.* **1970**, *92*, 4538.

(17) Krebs, B. *Angew. Chem., Int. Ed. Engl.* **1969**, *8*, 146.

If this line of reasoning is followed, the lack of bond alternation in the d^6–d^6–d^6 case arises because its d-block orbitals are fully occupied by the 18 d electrons. As a result, any stabilization of the bonding electron in σ_1' and π_1' in the $\theta_1 \neq \theta_2$ direction is countereacted by a destabilization of the antibonding electrons in σ_3' and π_3'. This is also the root cause of the shift in the optimum geometry to an angle smaller than 86° in the $\theta_1 = \theta_2$ direction.

There is still one fact we need to understand, the origins of the double minimum in the d^4–d^4–d^4 and d^5–d^5–d^5 cases, one with a uniform MM distance and the other with unequal MM distances. The first point to clarify is the formation of the symmetric ($\theta_1 = \theta_2$) minimum. Let us discuss it with respect to the d^4–d^4–d^4 case.

Returning to Figure 2, one sees that in the $\theta_1 = \theta_2$ direction, as one moves from the low-θ regime to the high-θ regime, there occurs an avoided crossing in the d^4–d^4–d^4 configuration. Two electrons that initially occupy σ_3 end up being in π_1 owing to σ_3–π_1 orbital crossing. This orbital crossing occurs at a region where σ_3 starts to rise sharply ($\theta_1 = \theta_2 \approx 85°$ Figure 2) and therefore results in a barrier at the locus of avoided crossing. This avoided crossing indeed leaves evidence in the energy surface of d^4–d^4–d^4. Our calculations show that the energy curve in a slice along the $\theta_1 = \theta_2$ direction exhibits a double minimum, one at $\theta_1 = \theta_2 = 80°$ and the other at $\theta_1 = \theta_2 \approx 88°$. The second is very close to the original d^0–d^0–d^0 minimum, and the two local minima are separated by a barrier at $\theta_1 = \theta_2 \approx 85°$, which is the locus of orbital crossing.

Let us start an excursion from the symmetric minimum at $\theta_1 = \theta_2 = 80°$, in the $\theta_1 \neq \theta_2$ direction. Looking back at Figure 7, one finds that the easiest way of excursion would be to keep one of the angles at 80° while increasing the other. Going in this direction leads again to avoided crossing in the d^4–d^4–d^4 configuration. One starts out with an occupied σ_3 orbital (at $\theta_1 = \theta_2 = 80°$; see Table I), which is being vacated along the direction $\theta_2 = 80°$, $\theta_1 > 80°$ (see Table I) and replaced by π_1'. The σ_3'–π_1' avoided crossing occurs at $\theta_1 \approx 85°$ ($\theta_2 = 80°$), where again, σ_3' rises steeply in energy. Since the d^0–d^0–d^0 curve is flat in this direction ($\theta_2 = 80°$, $\theta_1 > 80°$), the orbital crossing leaves its mark as a barrier separating the symmetric minimum at $\theta_1 = \theta_2 = 80°$ and the asymmetric one at $\theta_1 = 97°$, $\theta_2 = 80°$.

These considerations can be verified by a careful inspection of the d^4–d^4–d^4 surface.[18] The surface exhibits a barrier at $\theta_1 = 85°$, $\theta_2 = 80°$, which separates the two minima. This barrier coincides exactly with the locus of orbital crossing in the d block, at $\theta_1 = 85°$, $\theta_2 = 80°$. This coincidence arises because the core energy (d^0–d^0–d^0) is relatively flat in this direction and therefore it retains the memory of the orbital crossing as a barrier, consequently preserving the symmetric minimum at $\theta_1 = \theta_2 = 80°$ by surrounding it with energy barriers. The generation of a barrier between the symmetric and asymmetric minima is shown in Figure 9 as an interplay of the core energy and the avoided crossing in the d block. Figure 9 projects that the condition for *preserving a symmetric minimum in the M_3X_{14} trimers is a flat core energy and a significant orbital crossing, in the $\theta_1 \neq \theta_2$ asymmetric direction.* These two conditions are met also in the d^5–d^5–d^5 case, in which again the σ_3 orbital is crossed (by δ_1) in a region where it rises steeply ($\theta \approx 88°$). However, now the symmetric minimum is more stable than the asymmetric one, whereas in the d^4–d^4–d^4 case the two minima are approximately of the same energy.

Can we conclude from the foregoing discussion that for every d^4–d^4–d^4 and d^5–d^5–d^5 case there should coexist two isomers, one symmetric ($\theta_1 = \theta_2$) and high spin and the other asymmetric ($\theta_1 \neq \theta_2$) and low spin? No, of course not. The barrier separating the two isomers in Figure 9 is phenomenological. It obtains from the fine balance between the flatness of the core energy and the significance of the orbital crossing. Whenever either one of these conditions is not met, only one isomer will exist, be it the symmetric one or the asymmetric one.

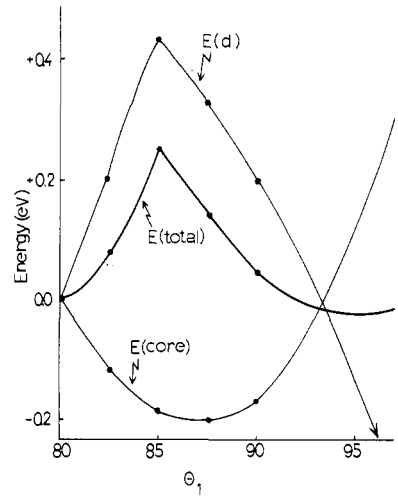

Figure 9. Formation of the barrier along the path separating the symmetric minimum ($\theta_1 = \theta_2 = 80°$) and the asymmetric minimum ($\theta_1 = 97°$, $\theta_2 = 80°$). The total energy, E(total), is a balance between the flat core energy, E(core), and the d-block energy, E(d), which arises from orbital crossing.

In summation, bond alternation ($\theta_1 \neq \theta_2$) arises since this is the only route along which the core energy (d^0–d^0–d^0) rises moderately, allowing the tendencies of the d block to be expressed. For low d counts in d^n–d^n–d^n, $n = 1$–3, this leads to structures with unequal MM distances ($\theta_1 \neq \theta_2$). For the higher d counts, $n = 4,5$, the orbital crossing in the d block forms a basis for existence of two isomers, one with equal MM distances ($\theta_1 = \theta_2$) and the other with unequal ones. For $n = 6$, the completely filled d block shows no tendency for bond alternation and therefore only a symmetric structure ($\theta_1 = \theta_2$) obtains.

C. Survey of Experimental Data. Oligomers like **4** are not known.[19,20] Therefore, a direct examination of our results, before they are projected onto polymers, is not possible. We are aware that direct comparison of our results with structural data on polymers is not the ideal choice. There are naturally some worries that arise from the lack of collective interactions and translational symmetry in the oligomer, and a full-scale band calculation will be needed to substantiate our conclusions. However, in one-dimensional chains, with weak interchain coupling, the key structural features are determined by close-neighbor interactions[10,12e,f] and, hence, are already set at the oligomer stage. True, the M_3X_{14} oligomers will differ in details in comparison with their corresponding polymers, but one expects the main trends, within a series of oligomers, to carry over to the series of polymers, which are characterized by weak interchain coupling.

There are a few d^1 MX_4 (M = Nb, Ta; X = Cl, Br, I) complexes, most of which are monomers in the gas phase with

(18) The detailed energy mapping in the region 70–110° for all d counts is available from the authors.

(19) The linear metal–metal-bonded trimer $[Mn_3(CO)_{14}]^-$ has been reported by: Bau, R.; Kirtley, S. W.; Sorreil, T. N.; Winarko, S. *J. Am. Chem. Soc.* **1974**, *96*, 988.

(20) Acyclic trimers with bridging atoms, but with other stoichiometries, were reported by: (a) Dilworth, J. R.; Zubieta, J.; Hyde, J. R. *J. Am. Chem. Soc.* **1982**, *104*, 365. (b) Roundhill, D. M. *Inorg. Chem.* **1980**, *19*, 557. (c) Bullen, J. C.; Mason, R.; Pauling, P. *Ibid.* **1965**, *4*, 456. (d) Bino, A.; Cotton, F. A. *J. Am. Chem. Soc.* **1980**, *102*, 608. (e) Delphin, W. H; Wentworth, R. A. D.; Matson, M. S. *Inorg. Chem.* **1974**, *13*, 2553.

a C_{2v} structure.[1a] In the solid state they form one-dimensional polymers with very weak interchain coupling. The known structures are those of $NbCl_4$[1b,21] and of α-NbI_4,[6] which form trans edge-sharing polyoctahedra (**1**), $[NbX_2(\mu\text{-}X)_{4/2}]_\infty$. Both are diamagnetic (or weakly paramagnetic[1a]) and exhibit bond alternation with $\theta_1 = 102\text{–}106°$ and $\theta_2 = 82\text{–}83°$. Thus, while the actual degree of alternation is larger than in our results (Table I), the phenomenon of alternation is reproduced by our model system. For all the other d^1 polymers, $NbBr_4$[1,21b,22] $TaCl_4$,[23] $TaBr_4$,[23] and TaI_4,[23,24] the powder data suggest that they are isostructural with $NbCl_4$ and α-NbI_4. The diamagnetism or weak paramagnetism of these compounds supports the powder data that they are endowed with MM bond alternation.

Other d^1 polymers of the general formula $[MO_{2/2}(\mu\text{-}X)_{4/2}]_\infty$ (M = Nb, Ta) also exhibit bond alternation.[1b,c,25]

Single-crystal X-ray data are not available for d^2 MX_4 polymers, $[MX_2(\mu\text{-}X)_{4/2}]_\infty$. Our results (Table I) suggest that these polymers should exhibit even more pronounced bond alternation than the d^1 polymers. Powder data on α-$MoCl_4$,[1a,26] WCl_4,[27] WBr_4[27] suggest that these polymers are isostructural with $NbCl_4$ and α-NbI_4. This, together with their weak paramagnetism,[26-28] provides some support for our prediction.

Incidently, our results show that, even at the greatest degree of bond alternation ($\theta_1 = 70°$, $\theta_2 = 110°$), the highest occupied orbital of the d^2–d^2–d^2 trimer, δ_3' (Figure 7), is close in energy to the upper lying orbitals σ_2', π_2' and δ_2' (energy gap $\sim$0.2 eV). This suggests that d^2 polymers of the type $[MX_2(\mu\text{-}X)_{4/2}]_\infty$ are not likely to be closed shell owing to overlap of their electronic bands.[9a]

Other types of d^2 polymers, $MoOCl_2$ and $WOCl_2$, have structures analogous to that of $NbOCl_2$.[25] They are two-dimensional polymers that share common edges via bridging chlorines and show marked MM bond alternation.[1b,25a,29]

The d^3 polymers with known structures are those of $TcCl_4$[30] and $ReCl_4$,[31] which do not have the structure **1**. Thus, while $TcCl_4$ crystalizes as cis edge-sharing polyoctahedra ($[TcCl_2(\mu\text{-}Cl)_{4/2}]_\infty$), $ReCl_4$ is composed of face-sharing bioctahedra connected to each other by common corners, $[ReCl_2(\mu\text{-}Cl)_{3/2}(\mu\text{-}Cl)_{1/2}]_\infty$.

However, as suggested by the donor–acceptor picture of the bridge bonding (**20**),[11c] there are many modes of connectivity available to the monomers. This is indeed the impression that one gets upon witnessing the polymorphism in these polymers. There exist three NbI_4 isomers,[6] at least two $MoCl_4$ isomers,[26] two $OsCl_4$[7] isomers, two or more $ReCl_4$ isomers,[31] etc. This, together with the fact that neither Re[3d] nor Tc refrain from forming edge-sharing bioctahedra or polyoctahedra, makes it feasible that the trans edge-sharing polyoctahedra polymers of Re and Tc can, in fact, exist. These polymers, if found, are predicted, by our calculations, to exhibit bond alternation (Table I).

d^4 is the first d count that is predicted in our analysis to lead to polymers, $[MX_2(\mu\text{-}X)_{4/2}]_\infty$, with a uniform and long MM distance (Table I). Such a polymer indeed exists. It is the high-temperature form of $OsCl_4$, which has a long and uniform OsOs distance of 3.560 Å and is known to be paramagnetic.[7]

Our results also predict that a low-spin polymer with bond alternation is an alternative structure for d^4. The only other d^4 polymers known to us are the $Cr^{II}P_4$ and $Mo^{II}P_4$ three-dimensional polymers, but they are composed of cis edge-sharing MP_6 octahedra.[32] However, on the basis of the donor–acceptor concept (**20**) and the common polymorphism within the family, we envision that d^4 trans edge-sharing polymers with bond alternation will soon be found.

There are no d^5 polymers of the type $[MX_2(\mu\text{-}X)_{4/2}]_\infty$ (X = halide). The structures that are known are those of $Mn^{II}P_4$.[5] This compound crystallizes in three isomers, which are all complicated three-dimensional networks of atoms. However, in each, one can identify chains of MnP_6 octahedra that share common edges. The first isomer, 2-MnP_4, consists of trans edge-sharing polyoctahedra. The second isomer, 6-MnP_4, consists of tetramers of trans edge-sharing octahedra that share a cis edge with one another. The third isomer, 8-MnP_4, is made of trans edge-sharing tetramers that are connected via common corners.

Despite this great variation in their nature the isomers share one common feature, i.e., MnMn bond alternation within the trans edge-sharing octahedra segments, with $\theta_1 = 97°$ and $\theta_2 = 75°$. Thus, this is a case where both the d^5 chain and the d^5 oligomeric units share the same tendency toward bond alternation.

The only other known d^5 polymer is that of bis(diethyldithiocarbamato)manganese(II), which forms chains with uniform MnMn distances but with unequal Mn–S bond lengths in the bridge.[33] Thus, the d^5 $[MX_2(\mu\text{-}X)_{4/2}]_\infty$ polymer with a uniform MM distance, which is predicted in Table I to exist, is yet to be made.

The d^6 polymers of PtI_4, $PtCl_4$, and $PtBr_4$ are known.[34] However, their structures consist of cis edge-sharing polyoctahedra. The only known d^6 structure with trans edge-sharing octahedra is that of α-$Fe^{II}P_4$.[35] It is made of trans edge-sharing *trimers* that are connected via common corners. The trimers have a uniform and long MM distance ($\theta = 78°$, $r = 3.50$ Å) as predicted in Table I.

What about d^0 polymers? Such a one exists. This is the polymer of $ZrCl_4$,[17] but it is not the desired isomer. Thus, the trans edge-sharing d^0 $[MX_2(\mu\text{-}X)_{4/2}]_\infty$ polymer is still lacking to complete the jigsaw puzzle.

All in all, our predictions fare quite well with experimental data. We now turn to utilize the insight we have gained in order to tinker with structural features.

Summary: How Can One Stabilize Polymers with a Uniform MM Distance?

As we have mentioned in the Introduction, the chain polymers (**1**) are considered as potential one-dimensional conductors.[1c,9a] A uniform MM distance is an absolute necessity for efficient metallic conductivity, and therefore it is desirable to attempt the design of low-dimensional materials that exhibit this structural feature.

Why do these polymers tend to alternate? Our analysis projects that they do so because the d electrons *can take*

(21) (a) Taylor, D. R.; Calabrese, J. C.; Larsen, E. M. *Inorg. Chem.* **1977**, *16*, 721. (b) McCarley, R. E.; Trop, B. A. *Ibid.* **1963**, *2*, 540.
(22) Schäfer, H.; Dohmann, K. D. *Z. Anorg. Allg. Chem.* **1961**, *311*, 134.
(23) McCarley, R. E.; Boatman, J. C. *Inorg. Chem.* **1963**, *2*, 547.
(24) Rolsten, R. *J. Am. Chem. Soc.* **1958**, *80*, 2952.
(25) (a) Schnering, H. G.; Wohrle, H. *Angew. Chem., Int. Ed. Engl.* **1963**, *2*, 558. (b) Schäfer, H.; Siffing, E.; Geskin, R.; *Z. Anorg. Allg. Chem.* **1961**, *307*, 163.
(26) (a) Kepert, D. L.; Mandyczewsky, R. M. *Inorg. Chem.* **1968**, *7*, 2091. (b) Brown, T. M.; McCann, E. L., III *Ibid.* **1968**, *7*, 1227. (c) Larson, M. L.; Moore, F. W. *Ibid.* **1964**, *3*, 285.
(27) (a) Brown, T. M.; McCarley, R. E. *U.S.A.E.C.* **1964**, *IS-741*. (b) McCarley, R. E.; Brown, T. M. *Inorg. Chem.* **1964**, *3*, 1232.
(28) Klemm, W.; Steinberg, H. *Z. Anorg. Allg. Chem.* **1936**, *227*, 193.
(29) Tillack, J.; Kaiser, R.; Fisher, G.; Eckerlin, P. *J. Less-Common Met.* **1970**, *20*, 171.
(30) (a) Elder, M.; Penfold, B. R. *Inorg. Chem.* **1966**, *5*, 1197. (b) Knox, K.; Coffey, C. E. *J. Am. Chem. Soc.* **1959**, *81*, 5.
(31) Cotton, F. A.; DeBoer, B. G.; Mester, Z. *J. Am. Chem. Soc.* **1973**, *95*, 1159.
(32) Jeitschko, W.; Donohue, P. C. *Acta Crystallogr., Sect. B* **1972**, *B28*, 1893.
(33) Ciampolini, M.; Mengozzi, C.; Orioli, P. *J. Chem. Soc., Dalton Trans.* **1975**, 205.
(34) (a) Borderson, K.; Thiels, G.; Holle, B. M. *Z. Anorg. Allg. Chem.* **1969**, *369*, 154. (b) Pilbrow, M. F. *J. Chem. Soc., Chem. Commun.* **1972**, 270. (c) Thiele, G.; Woditsch, P. *Angew. Chem., Int. Ed. Engl.* **1969**, *8*, 672.
(35) Jeitschko, W.; Braun, D. J. *Acta Crystallogr., Sect. B* **1978**, *B34*, 3196.

Table II. Optimum Angles (θ_1, θ_2) for $[Nb_3Cl_{14}]^Z$ (Z = 0, 1−) and $[Nb_3Cl_8(CO)_6]^Z$ (Z = 7+, 4+, 1+, 2−, 5−, 8−, 11−, 14−)

entry no.	Z	d count	θ_1, deg	θ_2, deg
		I. $[Nb_3Cl_{14}]^Z$		
1.	0	$d^{1/3}$–$d^{1/3}$–$d^{1/3}$	86	86
2.	1−	$d^{2/3}$–$d^{2/3}$–$d^{2/3}$	88	88
		II. $[Nb_3Cl_8(CO)_6]^Z$		
3.	7+	d^0–d^0–d^0	85	85
4.	4+	d^1–d^1–d^1	85	85
5.	1+	d^2–d^2–d^2	84	84
6.	2−	d^3–d^3–d^3	86	86
7.	5−	d^4–d^4–d^4	86	86
8.	8−	d^5–d^5–d^5	96	82
9.	11−	d^6–d^6–d^6	80	80
10.	14−	d^7–d^7–d^7	79	79

advantage of the available low-energy exit route of the d^0 core (Figure 8). Therefore, bond alternation is not a necessary feature of these polymers. What one needs to do then to stop bond alternation is not to let the d electrons take advantage of this exit route.

There are two ways one can try. The first approach is well-known in the literature.[1c,36] It consists of partial oxidation of the chain. This should reduce the influence of the d electrons and therefore temper the tendency for bond alternation. To check it, we have calculated $[Nb_3Cl_{14}]^Z$, Z = 0, 1−, which have a total of one and two d electrons and therefore simulate, respectively, the partially oxidized cases $d^{1/3}$–$d^{1/3}$–$d^{1/3}$ and $d^{2/3}$–$d^{2/3}$–$d^{2/3}$. Their optimized geometries are shown in the first two entries of Table II. One can see that both levels of oxidation lead to a uniform MM distance.

However, since our results for d^1–d^1–d^1 tend to underestimate the degree of bond alternation, we can only conclude that partial oxidation will reduce the tendency for bond alternation of d^1 polymers. Albeit this approach has a limited utility and can not be used for higher d counts, as can be gleaned from Table I, *it can be utilized to check our predictions, e.g., by inducing bond alternation in a uniform d^4 polymer via its partial oxidation to d^{3+x} ($x < 1$).*

The second approach involves chemical substitution of the bridge or the axial ligands in a manner that will deemphasize the influence of the d-block electrons and, hence, will produce uniform polymers.

The experience with bridging compounds[11a-c] shows that acceptor substituents may do the job. First, the donor–acceptor conceptualization of the bridge bonding (**20**) suggests that such polymers should be stable if the bridge ligands are donors while the axial ligands are acceptors[11c] (or vice versa). Second, acceptor groups tend to delocalize the d orbitals away from the metal.[11a-c] As a result, the propensity of the d-block electrons toward bond alternation may not be sufficient to overcome the repulsive walls of the d^0 core (e.g., Figure 7) and therefore will either generate polymers with uniform MM bond distance or will reduce the extent of bond alternation.

In order to check this idea, we have optimized the geometries of the trimer $[Nb_3Cl_8(CO)_6]^Z$ in which all the axial ligands were replaced with carbonyls, as shown in **22**. The variable

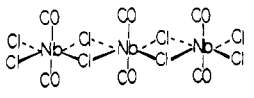

22

Z (=7+, 4+, 1+, 2−, 5−, 8−, 11−, 14−) serves to mimic metals with different d counts, for d^0–d^0–d^0 (Z = 7+) to d^7–d^7–d^7 (Z = 14−). The results are shown in Table II in entries 3–10. Evidently this mode of substitution (**22**) may indeed be a successful strategy for reducing the extent of bond alternation or may lead to polymers with uniform MM distances.

Trans edge-sharing polymers of this type (**22**) have in fact been inferred for $[Ru(CO)_2(\mu\text{-}X)_{4/2}]_\infty$, X = Cl, Br, I,[1a,37] but the exact structures are not known. The only analogous polymers with known structures are the d^6 and d^7 polymers $[M(py)_2(\mu\text{-}Cl)_{4/2}]_\infty$, M = Fe, Co (py = pyridine),[38] both of which are paramagnetic and have long (3.6 Å, $\theta \approx 86°$) and uniform MM distances.

Thus, acceptor axial ligands seem to be a partially successful solution to the bond alternation problem. However, for efficient conductivity one needs θ values larger than in Table II so that a large MM overlap will be established together with a uniform MM distance. Our analysis shows that the combination of axial ligands, which induce a uniform MM distance and bridging ligands with high ligand–ligand overlap repulsion (**21**), e.g., PR_2, SR, etc., which enforce high θ, may produce the desired effect. We are now pursuing the calculation of such possible models.

Acknowledgment. R.B. and S.S.S. are grateful to Professors J. E. M. Goldschmidt (deceased) and M. Albeck from the Department of Chemistry at Bar Ilan University for their encouragement and are grateful to them for making available the computer facilities. S.S.S. thanks Dr. P. Hofmann from Erlangen for making available his CDC version of the EH program. Special thanks are due to Mrs. Felicia Liber for the typing.

Appendix

Extended Hückel calculations with a weighted H_{ij} formula were used.[39] The parameters[40] are listed in Table III. The geometric parameters that were held fixed during the calculations of the model compounds are shown in Table IV.

Table III. Extended Hückel Parameters

atom	orbital	H_{ii}	orbital exponents[a] 1	2
Nb	5s	10.10	1.90	
	5p	6.86	1.85	
	4d	12.10	4.08 (0.6401)	1.64 (0.5516)
Cl	3s	30.00	2.033	
	3p	15.00	2.033	
C	2s	21.40	1.625	
	2p	11.40	1.625	
O	2s	32.30	2.275	
	2p	14.80	2.275	
H	1s	13.60	1.30	

[a] The coefficients in the double-ζ expansion of the d orbitals are given in parentheses.

Table IV. Bond Lengths for Model Compounds Nb_3Cl_{14}, $Nb_3Cl_8H_6$, and $Nb_3Cl_8(CO)_6$

bond	bond length, Å	bond	bond length, Å
Nb–Cl	2.474	C–O	1.180
Nb–C	2.000	Nb–H	1.700

Registry No. Nb_3Cl_{14}, 83682-15-9; Nb_3Cl_{10}, 83682-16-0; $Nb_3Cl_8H_6$, 83682-17-1; $Nb_3Cl_8(CO)_6$, 83682-18-2.

(36) For reviews, see, for example: (a) Miller, J. S.; Epstein, A. J. *Prog. Inorg. Chem.* **1976**, *20*, 1. (b) Keller, H. J., Ed. "Low-Dimensional Cooperative Phenomena"; Plenum Press: New York, 1974.

(37) Irving, R. J. *J. Chem. Soc.* **1956**, 2879.

(38) (a) Long, G. J.; Whitney, D. L.; Kennedy, J. E. *Inorg. Chem.* **1971**, *10*, 1406. (b) Dunitz, J. D. *Acta Crystallogr.* **1957**, *10*, 307. (c) Clarke, P. J.; Milledge, H. J. *Acta Crystallogr., Sect. B* **1975**, *B31*, 1543.

(39) Ammeter, J. H.; Bürgi, H. B.; Thibeault, J. C.; Hoffmann, R. *J. Am. Chem. Soc.* **1978**, *100*, 3686.

(40) (a) Nb H_{ii} values are from ref 11a. Nb orbital exponents are from: Basch, H.; Gary, H. B. *Theor. Chim. Acta* **1966**, *4*, 367. (b) The rest of the parameters are the usual extended Hückel parameters.